High-pressure Raman and x-ray study of the spin-frustrated pyrochlore $Gd_2Ti_2O_7$

Surajit Saha,[1] D. V. S. Muthu,[1] C. Pascanut,[2] N. Dragoe,[2] R. Suryanarayanan,[2] G. Dhalenne,[2] A. Revcolevschi,[2] Sukanta Karmakar,[3] Surinder M. Sharma,[3] and A. K. Sood[1,*]

[1]*Department of Physics, Indian Institute of Science, Bangalore 560012, India*

[2]*Laboratoire de Physico-Chimie de l'Etat Solide, ICMMO, CNRS, UMR8182, Bâtiment 414, Université Paris-Sud, 91405 Orsay, France*

[3]*Synchrotron Radiation Section, Bhabha Atomic Research Centre, Mumbai 400085, India*

(Received 29 April 2006; published 15 August 2006)

Pressure-dependent Raman and x-ray diffraction studies of spin-frustrated pyrochlore $Gd_2Ti_2O_7$ have been carried out at room temperature up to ~25 GPa and 34 GPa, respectively. A subtle distortion of the lattice at about 9 GPa is evidenced by Raman spectroscopy. X-ray results corroborate the distortion of the pyrochlore lattice at about the same pressure. Shell model lattice dynamical calculations were carried out in order to establish and understand the pressure dependence of Raman phonon frequencies. Our data may be relevant to the recent findings by Mirebeau *et al.* [Nature **420**, 54 (2002)] who observed magnetic correlations under high pressure in $Tb_2Ti_2O_7$, a frustrated spin-liquid system.

DOI: 10.1103/PhysRevB.74.064109 PACS number(s): 61.50.Ks, 78.30.−j, 61.10.−i

I. INTRODUCTION

Three-dimensional (3D) spin-frustrated systems, of which the rare earth titanates are typical examples, have been the subject of great interest in the last few years because of their novel properties exhibiting spin-ice and spin-liquid behavior.[1] Spin-ice has two spins pointing outward and two spins pointing inward, analogous to the water ice which has a tetrahedral building block with hydrogen atoms at the four vertices and oxygen at the center having two protons away from the oxygen atom and two close to it. Again analogous to the ordinary liquids, spin-liquid has only short-range correlation and no long-range interaction down to very low temperatures. As a result of the puzzling quantum fluctuations that exist down to very low temperatures, several theoretical and experimental investigations have been undertaken in the last two decades to understand the behavior of spins in these frustrated systems. The pyrochlore lattice contains magnetic rare-earth ions that are located at the vertices of tetrahedra in the structure and hence, the resulting antiferromagnetic interactions lead to geometrical frustration.[2] Ferromagnetic interactions can also give rise to spin frustration (spin-ice) as observed in $Ho_2Ti_2O_7$ and $Dy_2Ti_2O_7$.[3] Basically, frustrations develop when a spin system cannot minimize its ground-state energy by minimizing its spin-spin interactions. The pyrochlore structure belongs to the $Fd3m$ (O_h^7) space group with an $A_2B_2O_6O'$ stoichiometry. Following Wyckoff notations, in this structure the A^{3+} and the B^{4+} ions occupy, respectively, the 16*c* and the 16*d* sites, whereas O oxygen is at the 48*f* and O′ oxygen is at the 8*b* sites. The cubic unit cell consists of a lattice made of BO_6 octahedra and A_4O' tetrahedra. Due to this special structure, the interplay between spins and lattice has a significant role in the novel properties of these frustrated geometries. The study presented here focuses on one of these systems, namely, gadolinium titanate ($Gd_2Ti_2O_7$).

$Gd_2Ti_2O_7$ is a highly frustrated dipolar Heisenberg antiferromagnet, which undergoes a transition to a long-range antiferromagnetically ordered state at 0.97 K,[4] unlike spin-liquid and spin-glass states where the crystal field anisotropy on the A^{3+} cations plays an important role in ground-state selection. Neutron scattering experiments carried out on the spin-liquid $Tb_2Ti_2O_7$ suggest that there is a delicate balance among exchange coupling, crystal field and dipolar interactions which gives rise to significant quantum fluctuations even at very low temperatures.[1,5] But a pressure of about 8.6 GPa destroys this delicate balance and hence reduces frustration. This is believed to be the origin of the development of magnetic correlations at high pressure and low temperature (~1.5 K). Another possibility of reduction of the spin frustration can be the distortion of the pyrochlore lattice taking place at high pressures. The aim of the present high-pressure Raman experiment is to examine if pressure can induce structural distortions/transformations in $Gd_2Ti_2O_7$, which is an isostructural compound of $Tb_2Ti_2O_7$. Another motivation comes from the fact that the spin-spin exchange interactions in magnetic systems depend on lattice parameters (bond distances) which can be varied by pressure and can be probed by Raman spectroscopy, which is indeed a very powerful technique to probe the spin-lattice coupling in magnetic systems.[6] After the completion of our experiment, we came across a study which shows that $Sm_2Ti_2O_7$ picks up anion disorder above 40 GPa and $Gd_2Ti_2O_7$ at about 38 GPa and becomes amorphous above 51 GPa.[7,8] The focus of our work is a possible transition in $Gd_2Ti_2O_7$ at lower pressures.

II. EXPERIMENTAL DETAILS

Stoichiometric amounts of Gd_2O_3 (99.99%) and TiO_2 (99.99%) were mixed thoroughly and heated at 1200 °C for about 15 h. The resulting mixture was well grounded and isostatically pressed into rods of about 8 cm long and 5 mm diameter. Rods were sintered at 1400 °C in air for about 72 h. This procedure was repeated until the compound $Gd_2Ti_2O_7$ was formed, as revealed by powder x-ray-diffraction analysis. Using such rods, single crystals of $Gd_2Ti_2O_7$ were grown by a floating zone method using an infrared image furnace. Small cylindrical samples were cut from the resulting single crystal boules and were oxygen annealed at 1100 °C for a period of 100 h. X-ray diffraction,

carried out on powder obtained by crushing part of a single crystalline sample indicated a pure pyrochlore phase. Another part of the crystal was examined by scanning electron microscope equipped with an energy dispersive x-ray analyzer. The composition of the sample was found to be very close (within 1% accuracy) to that of the starting composition. Several small crystals cut from the grown boules were checked by x-ray Laue photographs in order to determine their orientation. Magnetization was measured on a piece of an oxygen-annealed single crystal in a field of 1 T in the 2–300 K temperature range. A paramagnetic behavior was found with no indication of any magnetic transition in this temperature range. The value of the Curie-Weiss temperature was found to be around −10 K and that of the effective magnetic moment was around $8\mu_B$, in close agreement with reported values.[3]

High-pressure Raman experiments were carried out at room temperature up to ~25 GPa. A single crystalline $Gd_2Ti_2O_7$ sample was placed in a hole of ~200 μm diameter drilled in a preindented stainless-steel gasket of a Mao-Bell-type diamond anvil cell with a mixture of 4:1 methanol and ethanol as the pressure transmitting medium. Pressure was calibrated using the ruby fluorescence technique.[9] Raman spectra were recorded in backscattering geometry using the 514.5 nm line of an argon ion laser and a SPEX RAMALOG Raman spectrometer equipped with a computer-interfaced photon counting system. $Gd_2Ti_2O_7$ was also studied up to 11.2 GPa in a gasketed Merrill-Basset diamond anvil cell with triple distilled water as the pressure-transmitting medium and a XY-DILOR micro-Raman spectrometer equipped with a liquid nitrogen cooled charge-coupled device (CCD). The Raman spectra were fitted with Lorentzian functions to determine the line shape parameters.

For the high-pressure x-ray experiments, single crystalline $Gd_2Ti_2O_7$ samples were crushed into fine powder which was loaded along with a few particles of gold, in a hole of ~120 μm diameter drilled in a preindented (~70 μm thick) tungsten gasket of a Mao-Bell-type diamond-anvil cell (DAC). The pressure-transmitting medium was a methanol and ethanol (4:1) mixture, similar to that used in the Raman studies. Pressure was determined from the known equation of state of gold.[10] High-pressure angle dispersive x-ray-diffraction experiments were carried out up to ~34 GPa on $Gd_2Ti_2O_7$ at the 5.2*R* (*XRD*1) beamline of the Elettra Synchrotron source (Italy) with monochromatized x rays (λ =0.690 12 Å). The diffraction patterns were recorded using a MAR345 imaging plate detector kept at a distance of ~20 cm from the sample. Two-dimensional (2D) imaging plate records were transformed into one-dimensional (1D) diffraction profiles by radial integration of the diffraction rings using the FIT2D software.[11] In order to understand the origin of the lattice vibrational modes, we have also performed shell-model calculations using the OpenPhonon code.[12]

III. RESULTS AND DISCUSSION

A. Raman spectra at ambient conditions

Group theory predicts the following representation for the zone-center optical vibrational modes of pyrochlore with space group $Fd3m$: $A_{1g}^R+E_g^R+2F_{1g}+4F_{2g}^R+3A_{2u}+3E_u+7F_{1u}^{IR}+F_{2u}^{IR}$, where R and IR represent Raman and infrared active modes, respectively. At ambient conditions, the Raman spectrum exhibits seven bands shown in the lowest panel of Fig. 1 and labeled as M_1 to M_7: M_1=215 cm^{-1}, M_2 =312 cm^{-1}, M_3=330 cm^{-1}, M_4=518 cm^{-1}, M_5=547 cm^{-1}, M_6=684 cm^{-1} and M_7=701 cm^{-1}. The position and relative intensities of these bands agree with reported spectra[13–15] which leads us to assign the modes M_1, M_2 and M_5 as F_{2g}, M_3 as E_g and M_4 as $A_{1g}+F_{2g}$. Apart from these five Raman active modes, two weak modes were also observed at 684 cm^{-1} (M_6) and 701 cm^{-1} (M_7). The origin of these modes, also seen in Refs. 13 and 14, is not clear at present but could be related to high frequency IR active modes.[14] In order to understand the various Raman active modes, we have performed lattice dynamical shell-model calculations. We will first discuss the results of the high-pressure experiments and try to interpret the results with the help of lattice dynamical calculations.

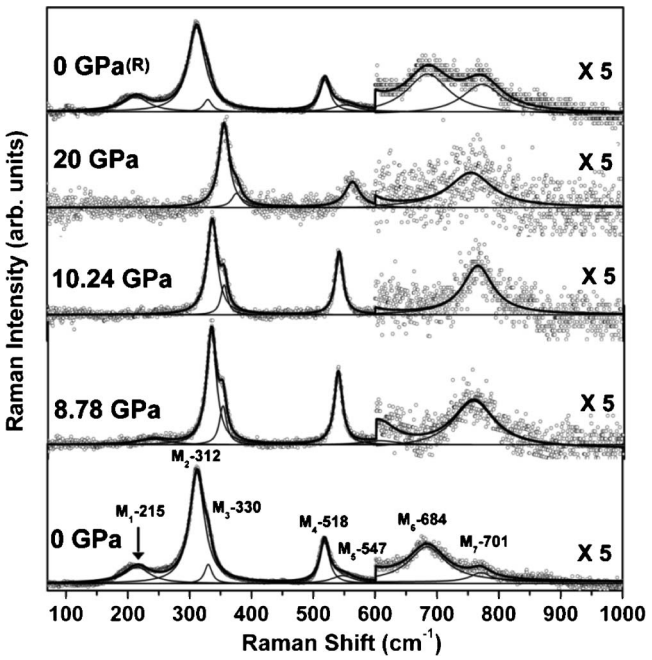

FIG. 1. Raman spectra at different pressures recorded during the increasing pressure run. The top panel is a Raman spectrum at ambient pressure after decompressing from ~24 GPa. Spectra at different pressures from 600–1000 cm^{-1} are zoomed by five times for clarity.

B. Pressure dependence of the vibrational modes

Raman spectra were recorded from 50 cm^{-1} to 1000 cm^{-1} at different pressures; a few of them are shown in Fig. 1. It can be very clearly seen that the intensity of the low frequency mode M_1 diminishes as pressure is increased and becomes difficult to observe beyond 9 GPa. When the sample is decompressed from ~25 GPa, this mode recovers, as seen in the top panel of Fig. 1. Another F_{2g} mode, M_5, is also affected by pressure and completely disappears above 9 GPa and reappears below that pressure on decompression.

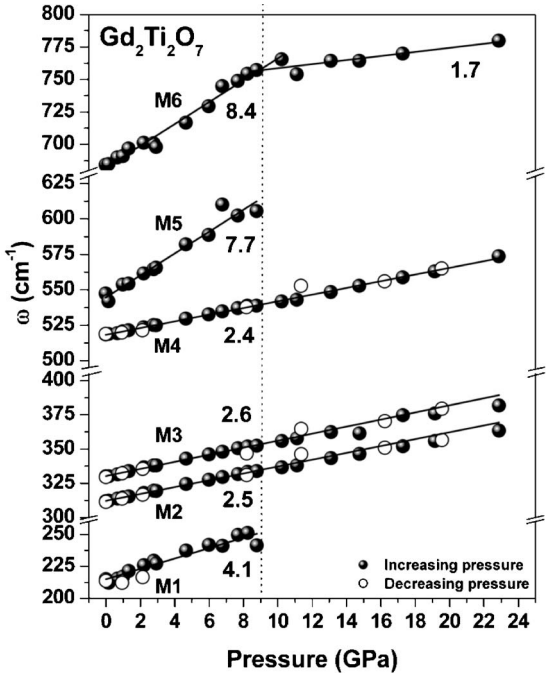

FIG. 2. Raman mode frequencies as a function of pressure during increasing and decreasing pressure runs. The pressure derivatives $(d\omega/dp)$ in cm^{-1}/GPa are indicated alongside the fitted lines to each mode.

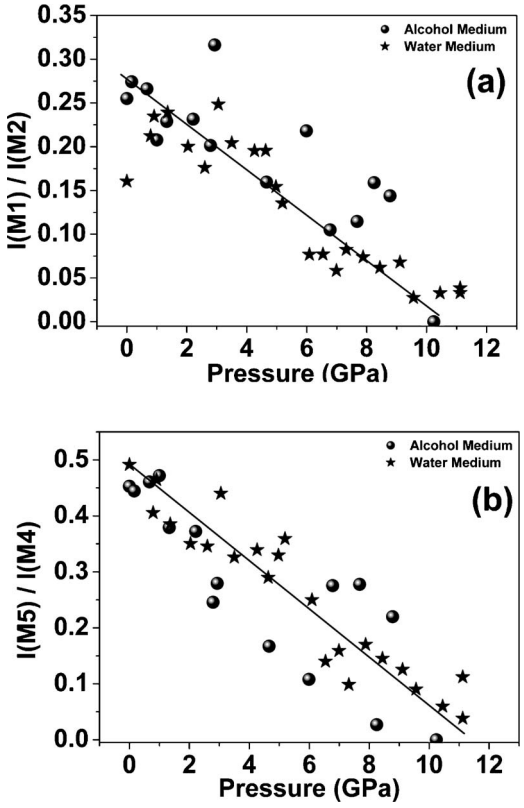

FIG. 3. The relative intensity of M_1 to M_2 and M_5 to M_4 modes, showing that the M_1 and M_5 modes disappear after about 9 GPa. Solid lines are guides to eye.

Out of the two weak modes not predicted by group theory, the M_6 mode shows a maximum change in frequency with pressure and a dramatic change in slope at ~9 GPa (Fig. 2). On the other hand, the strong modes, M_2 and M_4, do not show any change up to the maximum applied pressure (~25 GPa). The gradual decrease of the intensity of two Raman active modes M_1 and M_5, resulting in almost zero intensity at ~9 GPa, suggests a subtle structural change in the lattice, at this pressure. We note that the pressure-transmitting medium (methanol-ethanol mixture) remains hydrostatic just up to about 10 GPa. In order to ascertain if the nonhydrostatic nature of the medium plays any role in triggering the transition, we have also performed the high-pressure experiment with triple-distilled water as the pressure-transmitting medium. Water starts freezing above 1 GPa, making it a quasihydrostatic pressure medium. The pressure dependence of the modes is seen to be similar in both the pressure transmitting media. The value of the relative intensity of the M_1 mode with respect to that of the M_2 [Fig. 3(a)] mode and that of the M_5 to the M_4 [Fig. 3(b)] modes for the two pressure-transmitting media is the same. Therefore, we conclude that the transition at about 9 GPa is an intrinsic property of $Gd_2Ti_2O_7$. However, the possibility of a small contribution from the nonhydrostatic components, which can trigger the transition, cannot be completely ruled out. Therefore, conducting the experiment with helium as the pressure-transmitting medium will certainly give an insight to this issue.

From our lattice dynamical calculations and the known results,[15] the Raman active modes involve the movement of oxygen atoms only, where one of the F_{2g} modes, M_1, is solely due to $(8a)$ O′ vibrations and other modes (M_2, M_3, M_4, and M_5) are due to $(48f)$ O vibrations. The cations do not move. The low-frequency triply degenerate mode (M_1) is due to the vibration of the O′ oxygens, located at the center of the Gd_4O' tetrahedra [Figs. 4(a)–4(c)]. As discussed above, the intensity of this mode becomes negligibly small after 9 GPa and this may be attributed to a change in the O′ positions and/or a distortion of the tetrahedra. The other modes of vibrations are due to Gd-O stretching, O-Gd-O bending, O-O stretching, and O-Ti-O bending and stretching. These vibrations are coupled to each other in the octahedral lattice through the hexagonal crown. Another mode M_5 that disappears at the same pressure is a triply degenerate F_{2g} mode [Figs. 4(d)–4(f)] and we believe that a similar change in the anion position and/or a distortion in the octahedral lattice may be responsible for this. A more quantitative interpretation of the observed changes in the Raman spectra, as a function of pressure, is lacking at this time.

C. X-ray probing of the pressure effects

Figure 5 shows the x-ray diffraction patterns of $Gd_2Ti_2O_7$ at different pressures. Peaks marked G represent the diffraction peaks from gold (pressure marker) while the diffraction peaks from the tungsten gasket are denoted by W. All the diffraction peaks shift to higher angles with the increase of pressure and no phase transformation could be identified as implied by lack of emergence of any additional diffraction peaks up to the highest pressures, i.e., ~34 GPa. However,

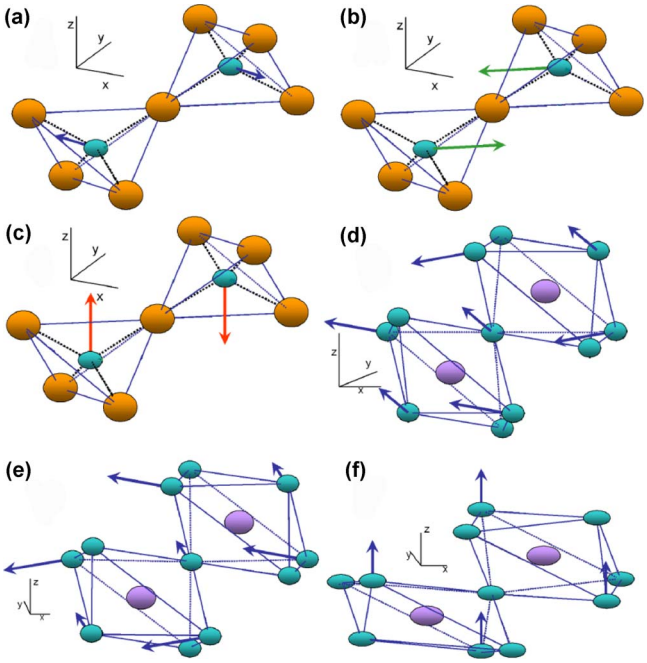

FIG. 4. (Color online) (a)–(c) Triply degenerate M_1 mode (215 cm^{-1}); (d)–(f) Triply degenerate M_5 mode (535.4 cm^{-1}).

as shown in Fig. 6, the pressure variation of the *d* spacings for some of the (strong) diffraction peaks displayed a change in slope at ~8.5 GPa. A similar change is also reflected in the pressure dependence of the cell constant (Fig. 7) and unit cell volume (Fig. 7, inset). Up to 8.5 GPa, a fit of the P-V data to the third order Birch-Murnaghan equation of state[16] gives $B=176\pm4$ GPa with $B'=6.9\pm1$. The same fit beyond

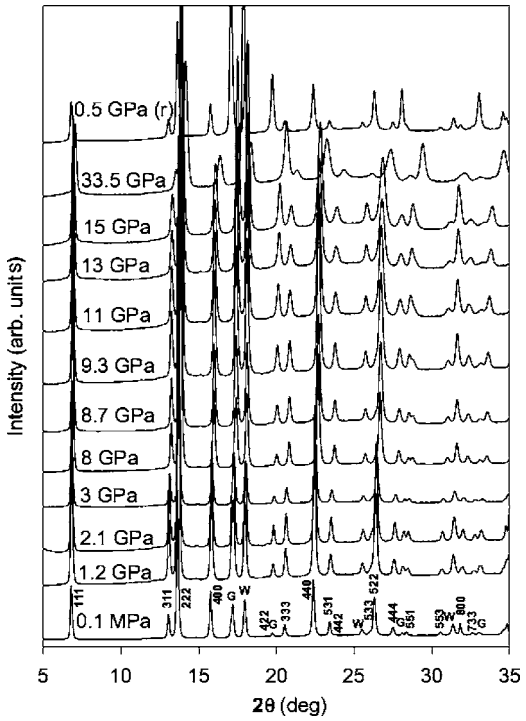

FIG. 5. X-ray spectra of $Gd_2Ti_2O_7$ at different pressures. *G* and *W* stand for gold and tungsten peaks, respectively.

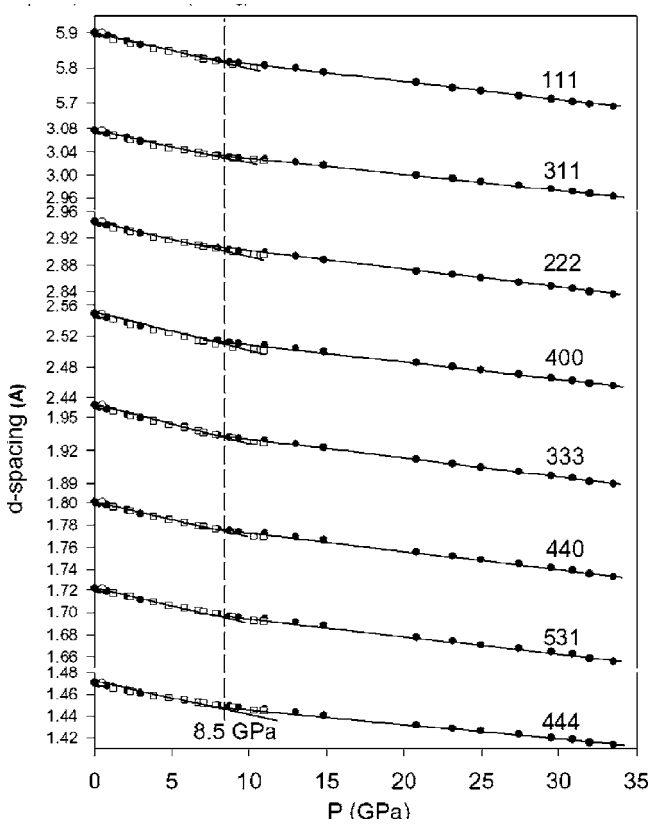

FIG. 6. Variation of the *d* spacing of a few lines of $Gd_2Ti_2O_7$ as a function of pressure.

8.5 GPa gives $B=208\pm8$ GPa with $B'=1\pm0.3$, implying that the bulk modulus increases by ~18% above 8.5 GPa. Since the observed change in the compressibility occurred at a pressure less than the pressure of the solidification of methanol ethanol mixture, it is likely that it arises from some intrinsic structural modification.

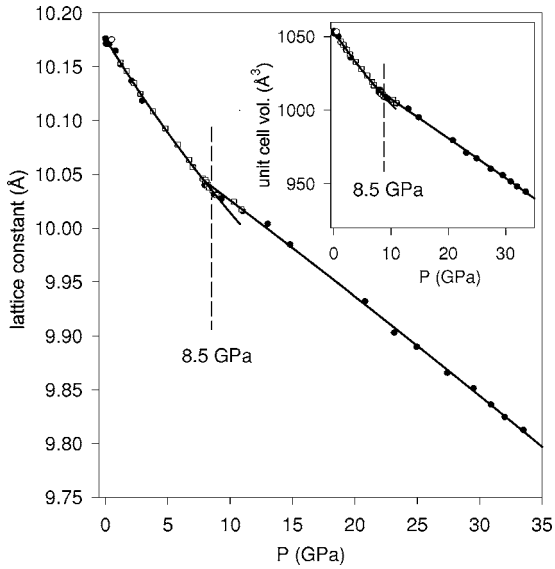

FIG. 7. Pressure-induced variation in the lattice constant of $Gd_2Ti_2O_7$. Variation of the unit cell volume with pressure is shown in the inset.

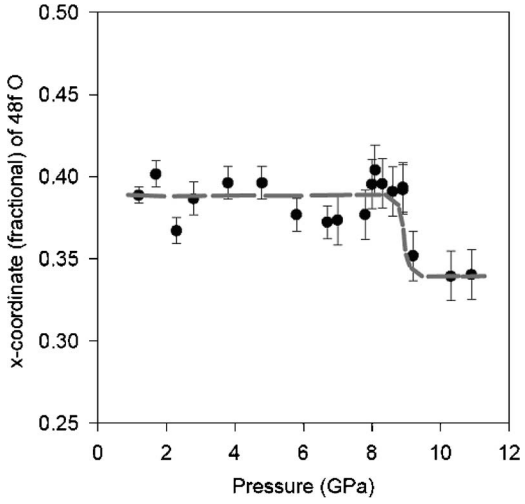

FIG. 8. Variation of the fractional coordinate of the 48*f* oxygen position (*x* coordinate) with pressure.

The pressure-induced variation in the fractional coordinate (x) of oxygen at the 48*f* site (the only adjustable positional coordinate in the pyrochlore structure) was deduced by Rietveld refinement, as implemented in the GSAS software.[17] The value of $x=0.39$ at ambient pressure is close to the reported values in the literature.[18] Figure 8 shows that this fractional coordinate underwent a sudden change (from ~0.39 to ~0.34) at ~9 GPa, implying a rearrangement of the TiO_6 octahedra. This might explain the change in compressibility of the $Gd_2Ti_2O_7$ pyrochlore at higher pressures. One may speculate that this rearrangement of the TiO_6 octahedra may also lead to the changes in the interatomic interactions leading to the disappearance of the two Raman active modes ($M1$ and $M5$) beyond 9 GPa.

D. Shell model calculations

Lattice dynamical calculations have been carried out for the Γ-point phonons of $Gd_2Ti_2O_7$, with a Coulomb potential for long-range interactions and a Born-Mayer-Buckingham (BMB) potential to account for the short-range interactions. The form of the BMB potential is

$$V_{kk'}(r_{ij}) = A_{kk'} \exp(-r_{ij}/R_{kk'}) - C_{kk'}/r_{ij}^6,$$

where r_{ij} is the distance between two ions i and j of species k and k', respectively. The values of the parameters $A_{kk'}$, $R_{kk'}$ and $C_{kk'}$ are tabulated in Table I. $C_{kk'}$ and $R_{kk'}$ are the strengths of the repulsive and the attractive potentials between the two shells, respectively, and $R_{kk'}$ is the range of interaction. Each ion consists of a charged core and a massless shell, such that the charges satisfy $Q^{Core}+Q^{Shell}=Q^{Formal}$. The shells are bound to the core with an elastic spring of spring constant K. The initial estimations for the parameters used in this calculation were taken from a calculation for $La_2Ti_2O_7$ (Ref. 019) and then the parameter values were tuned appropriately to match the calculated frequencies with our experimental results. A comparison of the calculated and experimental frequencies at ambient pressure is made in Table II. The eigenvectors of the normal modes, associated with Raman scattering, were confirmed by comparing with the reported eigenvectors.[15] The eigenvectors of only two F_{2g} modes, which disappear above 9 GPa, are shown in Fig. 4.

TABLE II. Raman frequencies (in cm^{-1}) from experimental data and shell model calculations.

$Gd_2Ti_2O_7$	$M_1(F_{2g})$	$M_2(F_{2g})$	$M_3(E_g)$	$M_4(A_{1g}/F_{2g})$	$M_5(F_{2g})$
Experimental	215	312	330	518	547
Calculations	214.9	311.6	327.5	518.4	535.5

In order to perform the pressure-dependent lattice dynamical calculations, we have used the values of the lattice parameters at different pressures obtained from our high-pressure x-ray diffraction results as inputs to the OpenPhonon program. The experimental values of the lattice constant from 0 to 8.5 GPa can be fitted to $a_P(Å)=a_0+bP$, where $a_0=10.1747$ Å, $b=-0.0165$ Å/GPa, and P is the pressure expressed in GPa. Intuitively, one can expect that as the pressure on the unit cell increases, the repulsive interaction between any two atoms will increase, thus increasing the range of interaction in the BMB potential. So, keeping $A_{kk'}$ and $C_{kk'}$ constant for all pressures, only $R_{kk'}$ is tuned so that the calculated values of the Raman active mode frequencies match with the experimental values. The calculations reveal that the range of interaction ($R_{kk'}$) increases with increasing pressure for the Gd-O, O-O, O-O′ and Ti-O potentials but not for Gd-O′ (Fig. 9). As mentioned above, the low frequency mode (M_1) is solely due to the vibration of the O′ atoms in the tetrahedral lattice. It is, therefore, interesting to observe that the $R_{kk'}$ in the Gd-O′ potential decreases with the increasing pressure and this may be related to the reduc-

TABLE I. Parameters of the shell-model calculations at ambient pressure.

Ion	Corecharge ($Q^{core}\|e\|$)	Shellcharge ($Q^{shell}\|e\|$)	Shell spring constant (K) (N/m)	Ionic pair	$A_{kk'}$ (eV)	$R_{kk'}$ (Å) (at 0 GPa)	$C_{kk'}$ (eV Å^6)
Gd	2.898	0.102	3554.0	Gd-O	1700.0	0.2842	0
				Gd-O′	1700.0	0.3142	0
Ti	2.907	1.093	3776.0	Ti-O	1256.2	0.2230	0
O	−1.616	−0.384	4483.3	O-O	22764.3	0.1490	27.89
O′	−1.914	−0.086	4188.8	O-O′	22764.3	0.1490	27.89

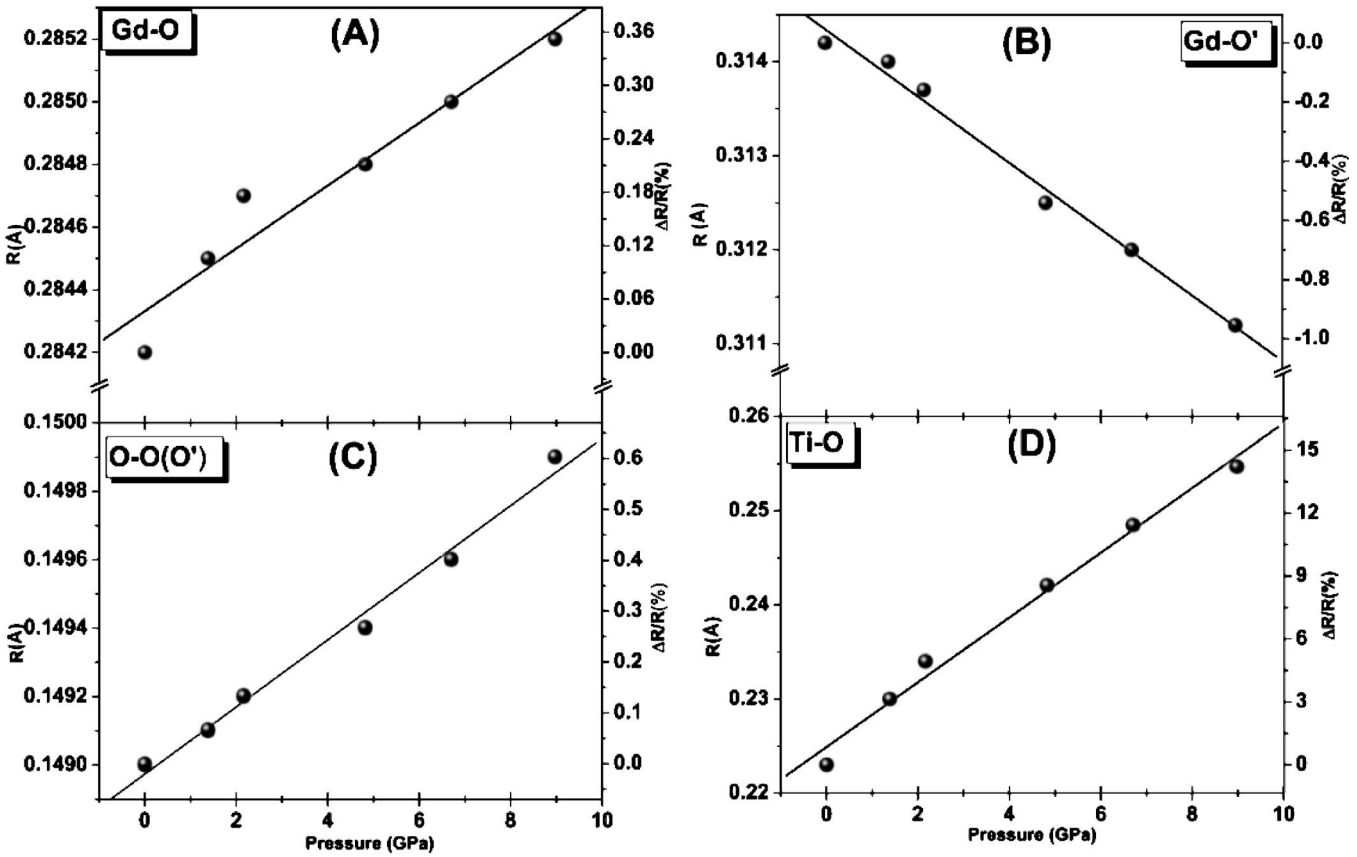

FIG. 9. Variation of the range of interaction ($R_{kk'}$) with pressure for different potentials obtained from lattice dynamical calculations. The $R_{kk'}$ of the Gd-O′ potential decreases with increasing pressure. The $R_{kk'}$ for O-O and O-O′ potentials are the same.

tion of the relative intensity of that mode with increasing pressure (Fig. 3) until it becomes negligibly small beyond 9 GPa. We see from Fig. 9 that the range of interaction ($R_{kk'}$) of the Ti-O potential undergoes a quite large change ($\sim$14%) in comparison with the $R_{kk'}$ of other potentials. Among all the three bending motions (O-Gd-O, O-Gd-O′ and O-Ti-O), the O-Ti-O is the dominant one[15] and we believe that this may have contributed significantly to the large change in the $R_{kk'}$ (Fig. 9) in the Ti-O potential under pressure.

IV. CONCLUSION

We have investigated the effect of pressure on the pyrochlore titanate $Gd_2Ti_2O_7$ through Raman scattering and x-ray diffraction. Our data suggest that the pyrochlore structure is stable up to $\sim$34 GPa. However, the observed changes indicate pressure induced distortions of the constituent polyhedra at $\sim$8.5 GPa. In particular, the intensities of the two Raman active modes M_1 and M_5 become negligibly small beyond 9 GPa, suggesting a subtle distortion of the lattice. Raman active modes incorporate the motions of anions only and hence the cationic motions are not reflected in Raman spectroscopic observations. It should be noted that in spin-frustrated systems, a significant pressure-induced structural distortion of the lattice may relieve the frustrations and initialize spin ordering. It will be interesting to explore whether such a scenario can be applicable to spin-liquid $Tb_2Ti_2O_7$, which will help us understand the appearance of magnetic correlations under pressure.[1] Similarly, high-pressure Raman and x-ray studies on the spin-ice systems such as $Ho_2Ti_2O_7$ and $Dy_2Ti_2O_7$ would be very rewarding.

ACKNOWLEDGMENTS

We thank the Indo-French Centre for Promotion of Advanced Research (IFCPAR), Centre Franco-Indien pour la Promotion de la Recherche Avancée (CEFIPRA) for financial support under Project No. 3108-1. A.K.S also thanks the Department of Science and Technology (DST), India for financial support. We acknowledge the help of Pallavi V. Teredesai in doing Raman experiments using water as the pressure-transmitting medium.

*Corresponding author. Electronic address: asood@physics.iisc.ernet.in

[1] I. Mirebeau, I. N. Goncharenko, P. Cadavez-Peres, S. T. Bramwell, M. J. P. Gingras, and J. S. Gardner, Nature (London) **420**, 54 (2002).
[2] M. A. Subramanian, G. Aravamudan, and G. V. Subba Rao, Prog. Solid State Chem. **15**, 55 (1983).
[3] John E. Greedan, J. Alloys Compd. **408**, 444 (2006).
[4] N. P. Raju, M. Dion, M. J. P. Gingras, T. E. Mason, and J. E. Greedan, Phys. Rev. B **59**, 14489 (1999).
[5] Isabelle Mirebeau and Igor Goncharenko, J. Phys.: Condens. Matter **16**, S653 (2004).
[6] E. Granado, A. Garcia, J. A. Sanjurjo, C. Rettori, I. Torriani, F. Prado, R. D. Sanchez, A. Caneiro, and S. B. Oseroff, Phys. Rev. B **60**, 11879 (1999).
[7] F. X. Zhang, B. Manoun, S. K. Saxena, C. S. Zha, Appl. Phys. Lett. **86**, 181906 (2005).
[8] F. X. Zhang and S. K. Saxena, Chem. Phys. Lett. **413**, 248 (2005).
[9] R. A. Forman, G. J. Piermarini, J. D. Barnett, and S. Block, Science **176**, 284 (1972).
[10] Agnes Dewaele, Paul Loubeyre, and Mohamed Mezouar, Phys. Rev. B **70**, 094112 (2004).
[11] A. P. Hammersley, S. O. Svensson, M. Hanfland, A. N. Fitch, and D. Hauserman, High Press. Res. **14**, 235 (1996).
[12] A. Miron, OpenPhonon Source Code, http://www.esrf.fr/computing/scientific
[13] M. T. Vandenborre and E. Husson, J. Solid State Chem. **50**, 362 (1983).
[14] M. T. Vandenborre, E. Husson, J. P. Chatry, and D. Michel, J. Raman Spectrosc. **14**, 63 (1983).
[15] H. C. Gupta, Sonal Brown, Neelima Rani, and V. B. Gohel, J. Raman Spectrosc. **32**, 41 (2001).
[16] F. Birch, J. Geophys. Res. **83**, 1257 (1978).
[17] Allen C. Larson and Robert B. Von Dreele, GSAS: General Structure Analysis System, Los Alamos National Laboratory, Los Alamos, NM, 1998, Report No. LAUR 86-748.
[18] N. J. Hess, B. D. Begg, S. D. Conradson, D. E. McCready, P. L. Gassman, and W. J. Weber, J. Phys. Chem. B **106**, 4663 (2002).
[19] Alain Chartier, Constantin Meis, William J. Weber, and L. Rene Corrales, Phys. Rev. B **65**, 134116 (2002).